High-Order Block Sliding-Mode Controller for a Synchronous Generator With an Exciter System

Alexander G. Loukianov, *Member, IEEE*, José M. Cañedo, *Member, IEEE*, Leonid M. Fridman, *Member, IEEE*, and Adolfo Soto-Cota, *Member, IEEE*

***Abstract*—This paper deals with the design of robust regulation for both angular speed stability enhancement and voltage in synchronous generator machines with an excitation control system. The designed controller is based on the block control technique combined with a sliding-mode (SM) control approach. The block control is used to design a nonlinear sliding manifold with the desired stability property. In order to attenuate the chattering effect which can appear in the presence of the exciter's unmodeled dynamics, a high-order SM algorithm and a robust exact differentiator are employed. The efficiency of the proposed controller, i.e., robustness and high accuracy, is verified via simulations.**

***Index Terms*—Excitation control system, power system control, power system stability, sliding-mode (SM) control, synchronous generator.**

I. Introduction

THE ROBUST controller design for excitations in a single synchronous generator connected to an infinite bus (see Fig. 1) remains one of the interesting problems in power system stabilization. The relevance of this controller lies in the fact that both the speed and the voltage are very important indexes determining the quality of the supplied energy to the consumers. Therefore, it is important to design robust excitation controllers that are capable of maintaining operation within adequate stability margins for these controlled outputs and an acceptable performance despite variations in the plant's parameters and external disturbances (i.e., externally applied load torques and momentary short circuits of the electrical output).

The excitation control system functionally consists of an exciter and an automatic voltage regulator [(AVR); see Fig. 1].

The aim of this regulator is to keep the terminal voltage equal to the prescribed value $V_{\rm ref}$. To provide the sufficient damping of multimodal oscillations, at all credible operating conditions, a supplementary control loop known as the power system stabilizer (PSS) is often added. It should be noted that the oscillations can be caused by a negative influence of the AVR in transient process [1], [2].

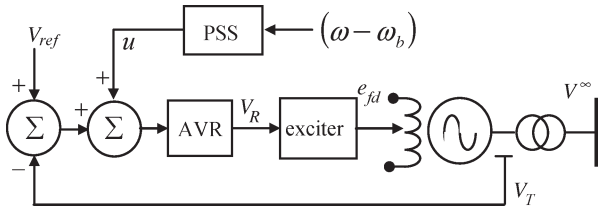

Fig. 1. Excitation control system.

Traditionally, the PSS design is based on linearized dynamic equations (see, for example, [1] and [3]), and consequently, only local stability for a specific operation point is achieved. Recently, to overcome the limitation of linear control, attention has been focused on the implementation of modern control techniques, e.g., adaptive linear control [4], [5], intelligent control such as fuzzy logic [6], [7] and neural networks [8], [9], control based on the direct Lyapunov method [2], adaptive control [10], feedback linearization (FL) technique [11], and others. In [12], it has been given a proposal of the nonlinear field voltage controller for synchronous generator stabilization via FL control. All the mentioned controllers provide larger stability margins with respect to traditional controllers. On the other hand, due to its low sensitivity to parameter variations and external disturbances, sliding-mode (SM) control [13] is a well-established control method for applications in nonlinear plants [14]–[17]. Based on this technique, an SM controller has been suggested in [18] for a single synchronous machine connected to an infinite bus and, in [19], for multimachine systems. The proposed first-order SM (FOSM) controller, however, can lose robustness in the presence of the exciter system's unmodeled dynamics with relative degree two, which were not considered in [18]. In fact, the exciter system dynamics are slow with respect to stator variables and fast with respect to mechanical and flux dynamics. In a continuous control scheme (see, for example, [3]), the effects of these fast dynamics rapidly decay since they are stable, and therefore, the exciter dynamics could be omitted. On the other hand, the unmodeled exciter dynamics can generate chattering in the power system with the FOSM controller (see, for example, [20]–[22]). This chattering effect is manifested as vibrations in the mechanical parts and undesirable heat losses, which lead to a low control accuracy. Therefore, the design of a bounded controller for the synchronous generator, keeping insensitivity with respect to perturbations, and the reduction of the chattering effect, despite

Manuscript received July 21, 2009; revised November 3, 2009; accepted January 5, 2010. Date of publication March 18, 2010; date of current version December 10, 2010. This work was supported by the Consejo Nacional de Ciencia y Tecnología, México, under Grant 46069 and by the Fondo de Cooperación Internacional en Ciencias y Tecnología UE–México, Grant 93302.

A. G. Loukianov and J. M. Cañedo are with the Centro de Investigación y Estudios Avanzados del Instituto Politécnico Nacional, Unidad Guadalajara 45010, México (e-mail: louk@gdl.cinvestav.mx; canedoj@gdl.cinvestav.mx).

L. M. Fridman is with the Department of Control and Robotics, National Autonomous University of Mexico (UNAM), México City 04510, México.

A. Soto-Cota is with the Departamento de Ingeniería Eléctrica, Instituto Tecnológico de Sonora, Obregón 85000, México (e-mail: adolfosoto@itson.mx).

Color versions of one or more of the figures in this paper are available online at http://ieeexplore.ieee.org.

Digital Object Identifier 10.1109/TIE.2010.2045319

the presence of the unmodeled exciter dynamics, becomes to be a challenging task.

This paper presents a novel approach to the stabilizer design for a single synchronous machine connected to an infinite bus in the presence of the exciter system dynamics. This approach is based on *block control technique* [23], combined with *high-order SM (HOSM)* algorithms [24]–[32]. At first, the block control technique is applied to design a nonlinear sliding manifold in such a way that an SM motion on this manifold is described by a desired linear system. Because the dynamics of the designed sliding variable have relative degree three (due to the presence of exciter dynamics in the system), then, the third-order SM algorithm is implemented to ensure the SM stability. The implementation of this algorithm needs the calculation of the sliding function and its first and second time derivatives. In the case of the synchronous generator's complex dynamics, direct calculations of these derivatives can result in a computationally expensive control algorithm. For this reason, a robust exact differentiator [26], [28] is employed.

This paper is organized as follows. Section II presents the synchronous generator's sixth-order model and exciter system dynamics. In Section III, a brief description of the FOSM and HOSM is given. In Section IV, the third-order SM controller with a robust exact differentiator is designed, and the closed-loop power system stability analysis is presented. Section V presents the simulation results. Section VI gives some conclusions.

Note that the stator currents are equal to the external network ones.

II. Model of Synchronous Generator

A. Basic Equations

The mathematical models for the synchronous generator are based on the mechanical and electric equilibrium equations (see [1] and [33]–[35]). The mechanical equilibrium equations for a synchronous generator are given by

$$\frac{d\delta}{dt} = \omega - \omega_b \tag{1}$$

$$\frac{d\omega}{dt} = \frac{\omega_b}{2H} t(T_m - T_e) \tag{2}$$

where δ is the power angle (in radians), ω is the angular velocity of the rotor (in radians per second), ω_b is the synchronous angular velocity (in radians per second), H is the inertia constant (in seconds), T_m is the mechanical torque [per unit (p.u.)], and T_e is the electromagnetic torque (p.u.). On the other hand, the electric equilibrium equations, affected by the Park transformations [33], [34], are expressed as

$$\boldsymbol{V} = \boldsymbol{R}\boldsymbol{i} + \frac{\omega}{\omega_b}\boldsymbol{G}\varphi + \frac{1}{\omega_b}\frac{d\varphi}{dt} \tag{3}$$

$$\varphi = \boldsymbol{L}\boldsymbol{i} \tag{4}$$

where t is the time in seconds, $\boldsymbol{V} = [\nu_d, \nu_q, \nu_f, 0, 0, 0]^{\mathrm{T}}$, $\boldsymbol{V}_g = [\nu_d, \nu_q]^{\mathrm{T}}$, $\varphi = [\varphi_d, \varphi_q, \varphi_f, \varphi_g, \varphi_{kd}, \varphi_{kq}]^{\mathrm{T}}$, and $\boldsymbol{i} = [i_d, i_q, i_f, i_g, i_{kd}, i_{kq}]^{\mathrm{T}}$; the variables $\boldsymbol{V}$, $\boldsymbol{i}$, φ, $\boldsymbol{R}$, and $\boldsymbol{L}$ represent the voltage, current, flux linkage, resistance matrix, and inductance matrix, respectively

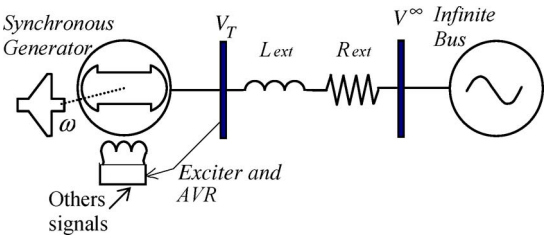

Fig. 2. Single machine—infinite bus.

$$\boldsymbol{R} = \mathrm{diag}(-r_s, -r_s, r_f, r_g, r_{kd}, r_{kq})$$

$$\boldsymbol{G} = \begin{bmatrix} 0 & -1 & 0 & 0 & 0 & 0 \\ 1 & 0 & 0 & 0 & 0 & 0 \\ 0 & 0 & 0 & 0 & 0 & 0 \\ 0 & 0 & 0 & 0 & 0 & 0 \\ 0 & 0 & 0 & 0 & 0 & 0 \\ 0 & 0 & 0 & 0 & 0 & 0 \end{bmatrix}$$

$$\boldsymbol{L} = \begin{bmatrix} -L_d & 0 & L_{md} & 0 & L_{md} & 0 \\ 0 & -L_q & 0 & L_{mq} & 0 & L_{mq} \\ -L_{md} & 0 & L_f & 0 & L_{md} & 0 \\ 0 & -L_{mq} & 0 & L_g & 0 & L_{mq} \\ -L_{md} & 0 & L_{md} & 0 & L_{kd} & 0 \\ 0 & -L_{mq} & 0 & L_{mq} & 0 & L_{kq} \end{bmatrix}.$$

The equation for the electromagnetic torque is expressed in terms of the currents and fluxes as

$$T_e = \varphi_d i_q - \varphi_q i_d. \tag{5}$$

B. External Network

The synchronous machine is connected to an infinite bus through a transmission line; see Fig. 2.

The model of the external line after Park's transformations can be written as [36]

$$\boldsymbol{V}_T = L_{\mathrm{ext}} \frac{d\boldsymbol{i}_s}{dt} + \mathbf{F}(\omega)\boldsymbol{i}_s + V^{\infty}\boldsymbol{Y} \tag{6}$$

where $\boldsymbol{V}_T = \begin{bmatrix} \nu_d \\ \nu_q \end{bmatrix}$; $\boldsymbol{i}_s = \begin{bmatrix} i_d \\ i_q \end{bmatrix}$; $F(\omega) = 1/\omega_b \begin{bmatrix} R_{\mathrm{ext}} & -\omega L_{\mathrm{ext}} \\ \omega L_{\mathrm{ext}} & R_{\mathrm{ext}} \end{bmatrix}$

$$\boldsymbol{Y} = \begin{bmatrix} \sin\delta \\ \cos\delta \end{bmatrix}$$

L_{ext} and R_{ext} are the line inductance and line resistance, respectively, in p.u.; V^{∞} is the infinite bus voltage (p.u.) settled at 1; $\boldsymbol{i}_s$ is the current line (p.u.); $\boldsymbol{V}_T$ is the voltage at the generator; and δ is the generator's power angle (in radians). Note that the stator currents are equal to the external network ones.

C. State Space Model

From (1)–(6), neglecting the fast stator dynamics

$$\mu \frac{d\boldsymbol{i}_s}{dt} = F_z(\mathbf{x}_1, \mathbf{x}_2, \boldsymbol{i}_s)$$

where

$$F_z = \begin{bmatrix} c_{11}x_2x_4 + c_{12}x_2x_6 + c_{13}x_2i_q + c_{14}i_d + c_{15}\sin x_1 \\ c_{21}x_2x_3 + c_{22}x_2x_5 + c_{23}x_2i_d + c_{24}i_q + c_{25}\cos x_1 \end{bmatrix}$$

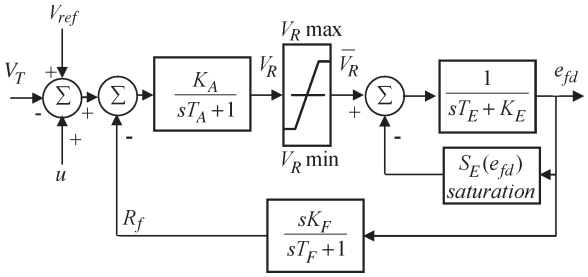

Fig. 3. Type 1 exciter control system.

and $\mu=1/\omega_b$, by setting $\mu=0$ and simplifying the aforementioned equations, we obtain the sixth-order power system model which describes the rotor's mechanical and electrical dynamics

$$\begin{bmatrix}\dot{\mathbf{x}}_1\\ \dot{\mathbf{x}}_2\end{bmatrix}=\begin{bmatrix}F_1(\mathbf{x}_1,\mathbf{x}_2,T_m,i_d,i_q)\\ F_2(\mathbf{x}_1,\mathbf{x}_2,i_d,i_q)\end{bmatrix}+\begin{bmatrix}B_1\\ 0\end{bmatrix}e_{fd} \tag{7}$$

$$\begin{bmatrix}i_d\\ i_q\end{bmatrix}=\begin{bmatrix}c_{14} & c_{13}\\ c_{23} & c_{24}\end{bmatrix}^{-1}\begin{bmatrix}c_{11}x_2x_4+c_{12}x_2x_6+c_{15}\sin x_1\\ c_{21}x_2x_3+c_{22}x_2x_5+c_{25}\cos x_1\end{bmatrix}:=\begin{bmatrix}h_1(\mathbf{x}_1,\mathbf{x}_2)\\ h_2(\mathbf{x}_1,\mathbf{x}_2)\end{bmatrix} \tag{8}$$

where $\mathbf{x}_1=(x_1,x_2,x_3)^{\mathrm{T}}=(\delta,\omega,\varphi_f)^{\mathrm{T}}$, e_{fd} is the exciter voltage, $\mathbf{x}_2=(x_4,x_5,x_6)^{\mathrm{T}}=(\varphi_g,\varphi_{kd},\varphi_{kq})^{\mathrm{T}}$, and

$$F_1=\begin{bmatrix}x_2-\omega_b\\ d_mT_m-[a_{21}x_3i_q+a_{22}x_4i_d+a_{23}x_5i_q+a_{24}x_6i_d+a_{25}i_di_q]\\ a_{31}x_3+a_{32}x_5+a_{33}i_d\end{bmatrix}$$

$$B_1=\begin{bmatrix}0\\ 0\\ b_3\end{bmatrix}\qquad d_m=\frac{\omega_b}{2H}$$

$$F_2=\begin{bmatrix}b_{11}x_4+b_{12}x_6+b_{13}i_q\\ b_{21}x_3+b_{22}x_5+b_{23}i_d\\ b_{31}x_4+b_{32}x_6+b_{33}i_q\end{bmatrix}.$$

The coefficients of (7) and (8) depend on the plant's parameters. A more detailed development of the system modeling can be found in several papers on power systems (see, for example, [1], [3], and [36]).

D. Exciter Control System

In this paper, we consider the typical IEEE Type 1 exciter system, which includes the continuously acting AVR and exciter. The block diagram for this system is shown in Fig. 3. A comprehensive description of this exciter system can be found in [1] and [37].

From the block diagram, we write the following equations:

$$T_E\frac{de_{fd}}{dt}=-(K_E+S_E(e_{fd}))\,e_{fd}+\overline{V}_R \tag{9}$$

$$T_A\frac{dV_R}{dt}=-V_R+K_AR_f+K_A(V_{ref}-V_T)+u \tag{10}$$

$$T_F\frac{dR_f}{dt}=-R_f-\frac{K_F(K_E+S_E(e_{fd}))}{T_E}\,e_{fd}+\frac{K_F}{T_E}V_R \tag{11}$$

where V_T is the generator terminal voltage, V_R is the regulator reference voltage setting, R_f is the rated feedback stabilizing transformer, T_E and K_E are the exciter's parameters, and T_F and K_F are the regulator stabilizing circuit's time constant and gain.

The output $\overline{V}_R$ of the regulator amplifier with the time constant T_A and gain K_A (which can be of the magnetic or electronic type) is bounded by saturation or power-supply restrictions; this is represented by the "nonwind" limits $V_{R\max}$ and $V_{R\min}$ (with $V_{R\min}=-V_{R\max}$) [1]

$$\overline{V}_R=\begin{cases}V_{R\max}, & \text{for } V_R\geq V_{R\max}\\ V_R, & \text{for } |V_R|t<V_{R\max}\\ V_{R\min}, & \text{for } V_R\leq V_{R\min}\end{cases}$$

and in this paper, it is approximated by the smooth function

$$\overline{V}_R(V_R)=\frac{2V_{R\max}}{\pi}\tan^{-1}\frac{\lambda\pi V_R}{2V_{R\max}}$$

where $\lambda=1$ is the slope of $\overline{V}_R(V_R)$. The block $S_E(e_{fd})$ in Fig. 3 represents the saturation function of the exciter. This function is defined by the Working Group IEEE as a multiplier of the exciter output e_{fd} to represent the increase in the excitation system because of saturation. A commonly used expression to approximate the exciter saturation $S_E(e_{fd})$ is the exponential function

$$S_E(e_{fd})=Ae^{Be_{fd}}$$

with $A=0.031$ and $B=6.93$ [1].

It is important to note that the actuator (9)–(11) already has a typical voltage control regulator. In this paper, a robust stabilizing controller design is considered, which replaces the typical stabilizing controller (PSS). The advantages of the proposed controller is that this controller can be implemented in the existing exciter control system with the AVR, changing only the PSS.

III. FOSM and HOSM Controller Designs

The main advantage of SM control is robustness in the presence of external and internal disturbances [13]. In Section III-A, the FOSM controller is presented, and in Section III-B, the HOSM control is described.

A. FOSM

Consider a class of nonlinear single-input–single-output systems

$$\dot{x}=f(x)+b(x)u+g(x,t)\qquad y=h(x)$$

which can be presented (possibly after a nonlinear transformation) in a nonlinear block controllable form (NBC form) [23] (or strict feedback form [39]) subject to uncertainty

$$\begin{aligned}\dot{x}_1&=f_1(x_1)+b_1(x_1)x_2+g_1(x_1,t)\\ \dot{x}_i&=f_i(\overline{x}_i)+b_i(\overline{x}_i)x_{i+1}+g_i(\overline{x}_i,t),\qquad i=2,\ldots,r-1\\ \dot{x}_r&=f_r(x)+b_r(x)u+g_r(x,t)\\ \dot{x}_j&=q_j(\zeta,\eta,t),\qquad j=r+1,\ldots,n\\ y&=x_1\end{aligned} \tag{12, 13}$$

where the state vector $x \in X \subset \Re^n$ is decomposed as $x = (x_1, \ldots, x_r, x_{r+1}, \ldots, x_n)^{\mathrm{T}} = (\zeta, \eta)^{\mathrm{T}}$, $\zeta = (x_1, \ldots, x_r)^{\mathrm{T}}$, $\eta = (x_{r+1}, \ldots, x_n)^{\mathrm{T}}$, $\overline{x}_i = (x_1, \ldots, x_i)^{\mathrm{T}}$, $i = 2, \ldots, r$, y and $u \in \Re$; f, b, and h are known to be sufficiently smooth vector valued functions of their arguments, g is a sufficiently smooth and bounded vector valued function, and $b_i(\overline{x}_i) \neq 0$, $i = 1, \ldots, r$ for all $\overline{x} \in X$. We assume that f and b are known, while g is an uncertain term which is composed by plant parameter variations and external disturbances. We further assume the following.

A1) The function $q(\zeta, \eta, t) = (q_{r+1}(x,t), \ldots, q_r(x,t))^T$ is globally Lipshitz in (ζ, η).

A2) The equilibrium point $\eta = 0$ of the residual dynamics

$$\dot{\eta} = q(0, \eta, t)$$

is globally uniformly asymptotically stable.

The general SM design procedure is the following. First, the output tracking error is defined as

$$z_1 = x_1 - y_{\mathrm{ref}} =: \varphi_1(x_1, t) \tag{14}$$

where y_{ref} is a reference signal. Then, using a block control linearizing transformation [23]

$$\begin{aligned} z_2 &= b_1(x_1)x_2 + f_1(x_1) + k_1\varphi_1(x_1,t) - \dot{y}_{\mathrm{ref}} =: \varphi_2(\overline{x}_1, t) \\ z_{i+1} &= \tilde{b}_i(\overline{x}_i)x_{i+1} - \tilde{f}_i(\overline{x}_i) - k_i\varphi_i(\overline{x}_i, t) =: \varphi_{i+1}(\overline{x}_{i+1}, t), \\ & \qquad i = 2, \ldots, r-1 \end{aligned} \tag{15}$$

where $\tilde{f}_i = \sum_{j=1}^{i-1}[(\partial\varphi_i/\partial x_j)f_j + b_j x_{j+1}] + (\partial\varphi_i/\partial x_i)f_i + (\partial\varphi_i/\partial t)$, $\tilde{b}_i = \tilde{b}_{i-1}b_i$, and $\tilde{g}_i = \sum_{j=1}^{i}(\partial\varphi_i/\partial x_j)g_j$; it is possible to show (see Appendix) that the system (12) and (13) can be presented as

$$\begin{aligned} \dot{z}_i &= -k_i z_i + z_{i+1} + \tilde{g}_i(\overline{z}_i, t), \qquad i = 1, \ldots, r-1 \\ \dot{z}_r &= \tilde{f}_r(\tilde{z}_r, \eta) + \tilde{b}_r(\tilde{z}_r, \eta)u + \tilde{g}_r(\tilde{z}_r, \eta, t) \\ \dot{\eta} &= q(\tilde{z}_r, \eta, t) \end{aligned} \tag{16}$$

where $\tilde{z}_r = (z_1, \ldots, z_r)^{\mathrm{T}}$, $\overline{z}_i = (z_1, \ldots, z_i)^{\mathrm{T}}$, $k_i > 0$, $i = 1, \ldots, r-1$, and $\tilde{b}_r = b_1, b_2, \ldots, b_r$. Taking advantage of this system's structure and choosing $z_r = 0$ as a sliding manifold, the control law

$$u = -u_0 b_r^{-1}\mathrm{sign}(z_r)$$

under the condition $u_0 > |\tilde{f}_r(\tilde{z}_r, \eta) + \tilde{g}_r(\tilde{z}_r, \eta, t)|$ makes the sliding manifold $z_r = 0$ attractive.

If the unmatched uncertainty $\tilde{g}_i(\overline{z}_i, t)$, $i = 1, \ldots, r-1$ is bounded and assumptions A1 and A2 are met, then there exist $k_i > 0$, where $i = 1, \ldots, r-1$, such that the solutions of the $(n-1)$th order SM equation (SME)

$$\begin{aligned} \dot{z}_i &= -k_i z_i + z_{i+1} + \tilde{g}_i(\overline{z}_i, t), \qquad i = 1, \ldots, r-2 \\ \dot{z}_{r-1} &= -k_{r-1}z_{r-1} + \tilde{g}_r(\overline{z}_{r-1}, t) \\ \dot{\eta} &= q(\overline{z}_{r-1}, \eta, t) \end{aligned} \tag{17}$$

are uniformly ultimately bounded [18], [23], i.e., the equilibrium point $(\overline{z}_{r-1} = 0, \eta = 0)$ of the nominal part of the system (17) is practically stable.

Remark 1: A sliding variable s can also be selected as a linear function of the tracking error

$$\xi_1 = x_1 - y_{\mathrm{ref}}$$

and its derivatives

$$\xi_i = \dot{\xi}_{i-1}, \qquad i = 2, \ldots, r \tag{18}$$

calculated along the trajectories of the system (12) in the absence of uncertainties

$$s = a_1\xi_1 + \cdots + a_{r-1}\xi_{r-1} + \xi_r$$

where $a_i > 0$, $i = 1, \ldots, r-1$. Then, the FOSM controller

$$u = -u_0 b_r^{-1}\mathrm{sign}(s)$$

achieves SM motion on $s = 0$ in finite time. Now, the SME of reduced $(n-1)$th order can be derived as

$$\begin{aligned} \dot{\overline{\xi}}_i &= \xi_{i+1} + \overline{g}_i(\overline{\xi}_i, t), \qquad i = 1, \ldots, r-2 \\ \dot{\overline{\xi}}_{r-1} &= -a_1\xi_1 - \cdots - a_{r-1}\xi_{r-1} + \overline{g}_{r-1}(\overline{\xi}_{r-1}, t) \\ \dot{\eta} &= q(\overline{\xi}_{r-1}, \eta, t) \end{aligned} \tag{19}$$

where $\overline{\xi}_i = (\xi_1, \ldots, \xi_i)^{\mathrm{T}}$. The parameters $a_i > 0$, $i = 1, \ldots, r-1$ in the system (19) are selected such that the polynomial $s^{(r)} + a_{r-1}s^{(r-1)} + \cdots + a_2 s + a_1 = 0$ is Hurwitz, and then, the equilibrium point $(\overline{\xi}_{r-1} = 0, \overline{x}_{r+1} = 0)$ of the nominal system under assumptions A1 and A2, and bounded perturbation $\overline{g}_i(\overline{\xi}_{r-1}, t)$, $i = 1, \ldots, r-1$, is practically stable.

Remark 2: It can be noted that, in order to derive the block linearized transformation (15) or canonical variables (18), it is necessary to calculate the successive derivatives of $f_i(\overline{x}_i)$ and $b_i(\overline{x}_i)$, $i = 1, \ldots, r-1$, in (12), which results in a computationally expensive control algorithm. Moreover, to achieve robustness with respect to unmatched uncertainties $\tilde{g}_i(\overline{z}_i, t)$, $i = 1, \ldots, r-1$, in the system (17) [or $\overline{g}_i(\overline{\xi}_{r-1}, t)$, $i = 1, \ldots, r-1$, in the system (19)], the controller gains $k_i > 0$, $i = 1, \ldots, r-1$ (or $a_i > 0$, $i = 1, \ldots, r-1$) must be selected sufficiently high.

To solve these problems and achieve more deep decomposition of the system (16), an HOSM controller combined with a robust exact differentiator [25] will be applied in the next section. It will allow reducing the SME (17) [or (19)] order and achieving robustness of the closed-loop system with respect to unmatched perturbations. Moreover, this combined approach permits one to reduce a number of sensors since the only part of the state variable is needed be measurable.

B. Nonlinear Block Controller With HOSMs

Assume that the system (12) and (13) models both the plant and its actuator with the relative degrees k and q, respectively, so that $k + q = r$; the plant variables $(x_1, \ldots, x_k)$ and the first variable of the actuator x_{k+1} are admissible for the

measurement; and $\tilde{g}_i(\overline{z}_i, t)$, $i = k+1, k+2, \ldots, r-1$, is a sufficiently smooth function. Thus, choosing s_0 in (15)

$$s_0 =: z_{k+1} = \varphi_{k+1}(\overline{x}_{k+1}), \qquad 1 < k < r-2$$

as a sliding variable and then taking its successive derivatives, straightforward calculations give

$$\begin{aligned}
\dot{z}_i &= -k_i z_i + z_{i+1} + \tilde{g}_i(\overline{z}_i, t), \qquad i = 1, \ldots, k-1 \\
\dot{z}_k &= -k_k z_k + s_0 + \tilde{g}_k(\overline{z}_k, t) \\
\dot{s}_j &= s_{j+1}, \qquad j = 0, \ldots, q-2 \\
\dot{s}_{q-1} &= \tilde{f}_{q-1}(\overline{z}_k, \overline{s}_{q-1}, t) + \tilde{b}_{q-1}(\overline{z}_k, \overline{s}_{q-1}, \overline{x}_{r+1} t)u \\
&\quad + \tilde{g}_{q-1}(\overline{z}_k, \overline{s}_{q-1}, \eta, t) \\
\dot{\eta} &= q(\overline{z}_k, \overline{s}_{q-1}, \eta, t)
\end{aligned} \tag{20}$$

where the variables $z_1, \ldots, z_k$ are defined in (16), $\overline{s}_{q-1} = (s_0, s_1 \ldots, s_{q-1})^{\mathrm{T}}$, and $\tilde{b}_{q-1} = b_{k+1} b_{k+2} \cdots b_r$. Denote

$$\begin{aligned}
N_{1,q} &= |s_0|^{p/q} \\
N_{i,q} &= \left(|s_0|^{p/q} + |s_1|^{p/(q-1)} + \cdots + |s_{i-1}|^{q-i+1)} \right)^{(q-i)/p}, \\
&\qquad i = 1, \ldots, q-1 \\
N_{q-1,q} &= \left(|s_0|^{p/q} + |s_1|^{p/q-1} + \cdots + |s_{q-2}|^{p/2} \right)^{1/p} \\
\psi_{0,q} &= s_0 \qquad \psi_{1,q} = s_1 + \beta_1 N_{1,q} \operatorname{sign}(\psi_{0,q}) \\
\psi_{i,q} &= s_i + \beta_i N_{i,q} \operatorname{sign}(\psi_{i-1,q}), \qquad i = 2, \ldots, q-1
\end{aligned} \tag{21}$$

where p are positive numbers $p \geq q$, and β_i, $i = 2, \ldots, q-1$, denotes the controller gains [25]. Then, assuming that, for some $C > 0$, $K_m > 0$, and $K_M > 0$, the following inequalities:

$$\begin{aligned}
\left| \tilde{f}_{q-1}(\overline{z}_k, \overline{s}_{q-1}, t) + \tilde{g}_{q-1}(\overline{z}_k, \overline{s}_{q-1}, \overline{x}_{r+1} t) \right| &\leq C \\
0 < K_m \leq \left| \tilde{b}_{q-1}(\overline{z}_k, \overline{s}_{q-1}, \overline{x}_{r+1} t) \right| &\leq K_M
\end{aligned}$$

hold, then, with properly chosen positive parameters α_0 and β_i, $i = 1, \ldots, q-1$, the controller

$$u = -\alpha_0 \operatorname{sign}\left[\psi_{q-1,q}(s_0, \ldots, s_{q-1}) \right] \tag{22}$$

provides for the *finite-time* attractivity of the SM on the *q-sliding set* [25]

$$s_j = 0, \qquad j = 0, \ldots, q-1. \tag{23}$$

The motion on the *q-sliding set* (23) is called *q-SM* (*qth-order SM*). The qth-order SM dynamics are described by the reduced $(n-q)$th-order SME

$$\begin{aligned}
\dot{z}_i &= -k_i z_i + z_{i+1} + \tilde{g}_i(\overline{z}_i, t), \qquad i = 1, \ldots, k-1 \\
\dot{z}_k &= -k_k z_k + \tilde{g}_k(\overline{z}_k, t) \\
\dot{\eta} &= q(\overline{z}_k, 0, \eta, t).
\end{aligned} \tag{24}$$

It is important to note that the HOSM controller (21) and (22), together with the $(q-1)$th-order robust exact differentiator [25], ensures the robustness of the closed-loop system (12)–(14) and (21) and (22) with respect to the matched uncertainty term $g_r(x, t)$, as well as the unmatched ones $g_i(\overline{x}_i, t)$, $i = k+1, \ldots, r-1$. Moreover, the parameter k in the system (20) can be adjusted to obtain a tradeoff between the controller complexity and robustness of the closed-loop system.

Remark 3: Note that the FOSM controller

$$u = -u_0 \tilde{b}_{q-1}^{-1} \operatorname{sign}(\sigma), \qquad \sigma = c_0 s_0 + \cdots + c_{q-2} s_{q-2} + s_{q-1} \tag{25}$$

can ensure the finite-time convergence of the state vector only to the manifold $\sigma = 0$, and the sliding motion on this manifold is governed by the SME of $(n-1)$th order

$$\begin{aligned}
\dot{z}_i &= -k_i z_i + z_{i+1} + \tilde{g}_i(\overline{z}_i, t), \qquad i = 1, \ldots, k-1 \\
\dot{z}_k &= -k_k z_k + s_0 + \tilde{g}_k(\overline{z}_k, t) \\
\dot{s}_j &= s_{j+1}, \qquad j = 0, \ldots, q-2 \\
\dot{s}_{q-2} &= -\sum_{\alpha=0}^{\alpha=q-2} c_\alpha s_\alpha \\
\dot{\eta} &= q(\overline{z}_k, \overline{s}_{q-1}, \eta, t).
\end{aligned} \tag{26}$$

If all the variables s_i, $i = 0, 1, \ldots, q-1$, in (25) are obtained from the differentiator, then the FOSM controller (25) would yield ideal robustness with respect to the uncertainties $g_i(\overline{x}_i, t)$, $i = k+1, \ldots, r$, similar to the HOSM controller (21) and (22). However, as it can be seen, the HOSM motion on the set (23) is described by the $(n-q)$th SME (24); thus, its stability is defined by with k eigenvalues $-k_1, \ldots, -k_k$ while the FOSM dynamics (26) are of the order $(n-1)$, and its local stability depends on $(k+q-1)$ eigenvalues. Therefore, if we try to implement SM of the order q in discrete time, we will obtain the precision $O(h^q)$ and $O(h)$ precision for the FOSM [25].

IV. HOSM Block Controller for Generator

In this section, to design a robust controller for the power system (7)–(11), we will first design the nonlinear set (23), and then, applying the HOSM approach, we will propose a discontinuous controller that ensures a desired SM motion on this set. It is important that the dynamics of the exciter system will not be taken into account in the control design procedure, while the quality of the FOSM controller for the synchronous generator in the presence of the unmodeled exciter dynamics will be saved even, in that case, some chattering can occur [19].

A. Nonlinear Sliding Set Design

To satisfy the control objective, which is the rotor angle stability, we define the control error as

$$\varepsilon_2 = x_2 - \omega_b. \tag{27}$$

Then, the system (7), (9)–(11) is rewritten as

$$\begin{aligned}
\dot{x}_1 &= \varepsilon_2 \\
\dot{\varepsilon}_2 &= f_2(\mathbf{x}_1, \mathbf{x}_2, T_m) - b_2(\mathbf{x}_1, \mathbf{x}_2) x_3 \\
\dot{x}_3 &= f_3(\mathbf{x}_1, \mathbf{x}_2) + b_3 e_{fd} \\
\dot{e}_{fd} &= f_e(e_{fd}) + b_e V_R \\
\dot{V}_R &= f_V(e_{fd}, V_R, V_{\text{ref}}, V_T, R_f) + b_V u \qquad (28) \\
\dot{R}_f &= f_R(e_{fd}, V_R, R_f) \\
\dot{\mathbf{x}}_2 &= \overline{F}_2(\mathbf{x}_1, \mathbf{x}_2) \qquad (29)
\end{aligned}$$

where $\overline{F}_2(x_1, x_2) = F_2(\mathbf{x}_1, \mathbf{x}_2, h_1(\mathbf{x}_1, \mathbf{x}_2), h_2(\mathbf{x}_1, \mathbf{x}_2))$, $f_2(\cdot) = d_m T_m - (a_{22} x_4 h_1(\cdot) + a_{23} x_5 h_2(\cdot) + a_{24} x_6 h_1(\cdot) + a_{25} h_1(\cdot) h_2(\cdot))$, $b_2 = a_{21} h_2(\cdot)$, $f_3(\cdot) = a_{31} x_3 + a_{32} x_5 + a_{33} h_1(\cdot)$, $f_e = -(K_E + S_E) e_{fd}/T_E$, $b_e = 1/T_E$, $b_V = 1/T_A$, $f_V(\cdot) = (1/T_A)[-V_R + K_A R_f + K_A(V_{\text{ref}} - V_T)]$, $f_R = -(1/T_F) R_f + (K_F (K_E + S_E)/T_F T_E) e_{fd} + (K_F/T_F T_E) V_R$, and $b_2(t)$ is a positive function of the time. The subsystem (29) describes the internal (uncontrolled) power system dynamics.

It can be noted that the excitation voltage e_{fd} was considered in [38] as the control input for the power system, and implementation of the designed discontinuous control algorithm in real life, i.e., in the presence of the additional exciter system dynamics (9)–(11), yields chattering.

The subsystem (28) has the NBC form (or strict feedback form), and the relative degree of this subsystem with respect to the control error ε_2 is equal to four. Therefore, it is possible to apply any FL technique: block control [23], backstepping [39], or exact linearization [40]. The direct implementation of these techniques leads to a computationally expensive control algorithm. To simplify the control algorithm, following the block control technique, we choose the desired linear dynamics for the control error ε_2 as

$$\dot{\varepsilon}_2 = -k_0 \varepsilon_2 + s_0. \qquad (30)$$

To achieve these dynamics, the virtual control x_3 in the second block of (28) is selected as

$$x_3 = b_2^{-1}[f_2(\mathbf{x}_1, \mathbf{x}_2, T_m) + k_0 \varepsilon_2 - s_0], \qquad k_0 > 0. \qquad (31)$$

Now, the sliding variable s_0 can be calculated from (31) as

$$s_0 = b_2(\mathbf{x}_1, \mathbf{x}_2) x_3 - f_2(\mathbf{x}_1, \mathbf{x}_2, T_m) - k_0(x_2 - \omega_b). \qquad (32)$$

Using (32), the projected motion equation of the system (28) and (29) on the subspace s_0 can be derived of the form

$$\dot{s}_0 = f_0(\mathbf{x}_1, \mathbf{x}_2, T_m) - b_0(\mathbf{x}_1, \mathbf{x}_2) e_{fd}$$

where $f_0(\cdot)$ is a continuous function, $b_0(\cdot) = b_3 b_2(\cdot)$, and $b_0(t) > 0$. Using s_0(32) and its derivatives

$$s_1 = \dot{s}_0 = f_0(\mathbf{x}_1, \mathbf{x}_2, T_m) + b_0(\mathbf{x}_1, \mathbf{x}_2) e_{fd} \qquad s_2 = \ddot{s}_0 \qquad (33)$$

as new variables, the subsystem (28) can be represented as

$$\begin{aligned}
\dot{x}_1 &= \varepsilon_2 \\
\dot{\varepsilon}_2 &= -k_0 \varepsilon_2 + s_0 \qquad (34) \\
\dot{s}_0 &= s_1 \\
\dot{s}_1 &= s_2 \\
\dot{s}_2 &= f_s(\mathbf{x}_1, \mathbf{x}_2, e_{fd}, V_R, V_T, V_{\text{ref}}, R_f, T_m) \\
&\quad - b_s(\mathbf{x}_1, \mathbf{x}_2) u \qquad (35)
\end{aligned}$$

where f_s is a continuous function, $b_s(\cdot) = b_3 b_2(\cdot)$, and $b_s(t)$ is a positive function of time. To enforce SM motion on $s_0 = 0$, $s_1 = 0$, and $s_2 = 0$, we select the third-order SM algorithm

$$\begin{aligned}
u &= -u_0 \text{sign}\left[\psi_{2,3}(s_0, s_1, s_2)\right], \\
&\qquad u_0 > 0; \quad \beta_2 > 0; \quad \beta_1 > 0 \\
\psi_{2,3}(s_0, s_1, s_2) &= s_2 + \beta_2 \left(|s_1|^3 + |s_0|^2\right)^{1/6} \\
&\quad \times \text{sign}\left(s_1 + \beta_1 |s_0|^{2/3} \text{sign}\, s_0\right). \qquad (36)
\end{aligned}$$

B. Stability Analysis

Assume that, in the admissible operation region $\Omega(\mathbf{x}_1, \mathbf{x}_2, T_m, V_{ref})$ for some $C_g > 0$, $K_{gm} > 0$, and $K_{gM} > 0$, the following inequalities hold:

$$\begin{aligned}
&|f_s(\mathbf{x}_1, \mathbf{x}_2, e_{fd}, V_R, V_T, V_{\text{ref}}, R_f, T_m)| \le C_g \\
&\qquad 0 < K_{gm} \le |b_s(\mathbf{x}_1, \mathbf{x}_2)| \le K_{gM}. \qquad (37)
\end{aligned}$$

Then, from [25], it follows that there exists a set of constants $u_0 > 0$, $\beta_1 > 0$, and $\beta_2 > 0$ such that the state vector of the closed-loop system (34)–(36) converges in finite time to the third-order SM set

$$s_0 = 0 \qquad s_1 = 0 \qquad s_2 = 0. \qquad (38)$$

The sliding motion on (38) is described by the reduced-order SME

$$\begin{aligned}
\dot{x}_1 &= \varepsilon_2 \qquad \dot{\varepsilon}_2 = -k_0 \varepsilon_2 \qquad (39) \\
\dot{z} &= -a_1 z - a_2 e_{fd,ss} + a_3 V_{R,ss} \\
\dot{\mathbf{x}}_2 &= \overline{F}_2(\mathbf{x}_1, \mathbf{x}_2) \qquad (40)
\end{aligned}$$

where $z = R_F$, $a_1 = 1/T_F$, $a_2 = K_F(K_E + S_E)/T_F T_E$, $a_3 = K_F/T_F T_E$, $e_{fd,ss}$, and $V_{R,ss}$ are the steady-state values of e_{fd} and V_R, respectively, on the set (38).

Note that the linear subsystem (39) with the desired eigenvalue $-k_0$ describes the transformed linearized mechanical dynamics on the sliding manifold $s_0 = 0$, while the subsystem (40) represents the rotor flux and exciter system internal dynamics on the sliding manifold $s_1 = 0$ and $s_2 = 0$. The second equation in (39), with $k_0 > 0$, is asymptotically stable; thus, $\lim_{t \to \infty} \varepsilon_2(t) = 0$, and the angle $x_1(t) = x_1(0) + \int_0^t \varepsilon_2(\upsilon) d\upsilon$ tends to a steady-state value $x_{1ss} = \delta_{ss}$ as the control error $\varepsilon_2(t)$ tends to zero. On the invariant subspace

$$\left\{\varepsilon_2 = 0, s_0 = 0, s_1 = 0, s_2 = 0, \mathbf{x}_2 \in R^3, z \in R\right\} \qquad (41)$$

the dynamics (40) are referred to as *zero dynamics*. To derive these dynamics, using (31) and (33), we calculate the excitation

flux x_3 and voltage e_{fd} values, respectively, on the invariant set (41) as

$$x_3 = -b_2^{-1}(\mathbf{x}_1, \mathbf{x}_2) f_2(\mathbf{x}_1, \mathbf{x}_2, T_m)$$
$$e_{fd} = b_0^{-1}(\mathbf{x}_1, \mathbf{x}_2) f_0(\mathbf{x}_1, \mathbf{x}_2, T_m). \quad (42)$$

Now, substituting the angle and speed steady-state values $x_1 = \delta_{ss}$ and $x_2 = \omega_b$ in (42) and then in subsystem (40) results in the following linear system with nonvanishing perturbation:

$$\dot{\eta}_z = A_z \eta_z + g_z(\eta_z, \delta_{ss}, \omega_b, T_m, e_{fd,ss}, V_{R,ss}) \quad (43)$$

where $\eta_z = \begin{bmatrix} z \\ \mathbf{x}_2 \end{bmatrix}$, $A_z = \begin{bmatrix} -a_1 & 0 \\ 0 & A_2 \end{bmatrix}$, $a_1 > 0$

$$A_2 = \begin{bmatrix} b_{11} - b_{13} a r_{21} c_{11} & -b_{13} a r_{22} c_{22} & b_{12} - b_{13} a r_{21} c_{12} \\ -b_{23} a r_{11} c_{11} & b_{22} - b_{23} a r_{12} c_{22} & -b_{23} a r_{11} c_{12} \\ b_{31} - b_{33} a r_{21} c_{11} & -b_{33} a r_{22} c_{22} & b_{32} - b_{33} a r_{21} c_{12} \end{bmatrix}$$

and $g_z(\mathbf{x}_2, \delta_{ss}, \omega_b, T_m, e_{fd,ss}, V_{R,ss})$ is a continuous function. Since A_z matrix in (43) is Hurwitz by virtue of rotor flux dynamics and g_z is a bounded function in $\Omega(\mathbf{x}_1, \mathbf{x}_2, T_m, V_{\text{ref}})$, then a solution to the zero dynamics (43) locally exponentially converges to a steady state $z = z_{ss}$ and $\mathbf{x}_2 = \mathbf{x}_{2ss}$ defined by a value of T_m.

C. Robust Exact Differentiator

The implementation of the proposed third-order SM controller requires real-time exact calculation of the s_1 and s_2 derivatives (33) that leads to a computationally expensive control algorithm. To avoid this problem and obtain these derivatives, an SM robust exact differentiator [25] is employed. We use the second-order robust exact differentiator defined by

$$\dot{z}_0 = \nu_0, \qquad \nu_0 = -\lambda_0 |z_0 - s_0|^{2/3} \operatorname{sign}(z_0 - s_0) + z_1$$
$$\dot{z}_1 = \nu_1, \qquad \nu_1 = -\lambda_1 |z_1 - \nu_0|^{1/2} \operatorname{sign}(z_1 - \nu_0) + z_2$$
$$\dot{z}_2 = -\lambda_2 \operatorname{sign}(z_2 - \nu_1) \quad (44)$$

where z_0, z_1, and z_2 are the estimates of the sliding variable s_0 and its derivatives s_1 and s_2, respectively. In [25], it was shown that there exists $\lambda_i > 0$, $i = 0, 1, 2$, such that the estimates z_0, z_1, and z_2 converge to the real variables s_0, s_1, and s_2, respectively, in finite time. These estimates are then implemented in controller (36) instead of the real variables.

It should be noted that only the generator speed dynamics were used to design the sliding surface $s_0 = 0$ (32) while the derivatives of s_0 were obtained via the HOSM differentiator (44); this does not require the knowledge of the exciter's (9)–(11) parameters.

V. Simulation Results

The proposed control algorithms were tested on the sixth-order model of a synchronous generator connected through a transmission line to an infinite bus, including the exciter control system (9)–(11). The simulations were done using MATLAB, the Euler integration method, and a fixed time step of 0.0001 s.

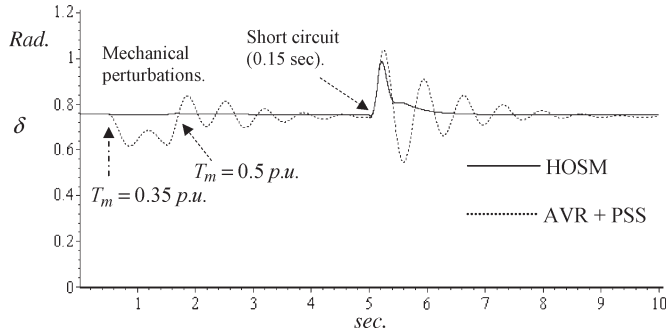

Fig. 4. Power angle during mechanical perturbation and short circuit. Performance comparison: HOSM controller versus AVR+PSS.

A. Nominal Parameters of Machine and Network

The data plate of the synchronous generator is 555 MVA, 0.9 p.f., 24 Kv, two poles, and three phases. The parameters of the synchronous machine and external network in p.u. are

$$T'_{do} = 8.0 \text{ s} \quad T'_{qo} = 1.0 \text{ s} \quad T''_{do} = 0.03 \text{ s}$$
$$T''_{qo} = 0.07 \text{ s} \quad \ell_a = 0.1 \quad H = 3.5 \text{ s}$$
$$L_d = 1.81 \quad L'_d = 0.3 \quad L''_d = 0.23$$
$$L_q = 1.76 \quad L'_q = 0.6 \quad L_{\text{ext}} = 0.1$$
$$R_{\text{ext}} = 0.001.$$

These values were used to calculate the parameters for the system (7) and (8).

B. Controller Parameters

The controller gains were chosen and adjusted to $u_0 = 0.2$ p.u., $k_0 = 10$, $\beta_2 = 2$, and $\beta_1 = 1$. The eigenvalues of matrix A_2 in (43) were calculated as $\lambda_a = -38.77$, $\lambda_b = -0.5024$, and $\lambda_c = -27.04$. The constants for the sliding differentiator were selected as $\lambda_0 = 125$, $\lambda_1 = 115$, and $\lambda_2 = 100$.

C. Results

To evaluate the efficiency of the proposed HOSM controller compared to the conventional PSS+AVR and the FOSM ones, several tests are now carried out under more significant perturbations in power systems.

Test A.1—Step Changes in T_m and Three-Phase Short Circuit With Plant Nominal Parameters; HOSM Controller Versus PSS+AVR: In the first test, starting in the steady-state condition $T_m(0) = 0.5$ p.u., the mechanical torque experienced first a step (-0.15) p.u. at $t = 0.5$ s, reaching 0.35 p.u., and then a step 0.15 p.u. at $t = 1.5$ s, reaching 0.5 p.u. Finally, a 150-ms three-phase short circuit at $t = 5$ s is applied at the transformer terminals. Figs. 4 and 5 show the angle and velocity responses. The solid line is the performance of the proposed HOSM controller, while the dotted line is the response of the classical PSS+AVR. The simulation results clearly indicate that the proposed HOSM controller provides better damping enhancement than the classical one. Figs. 6 and 7 show that, in spite of the strong disturbance, the terminal voltage and

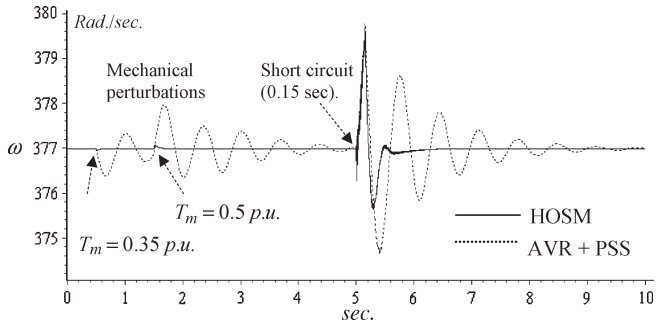

Fig. 5. Rotor velocity during mechanical perturbation and short circuit. Performance comparison: HOSM controller versus AVR+PSS.

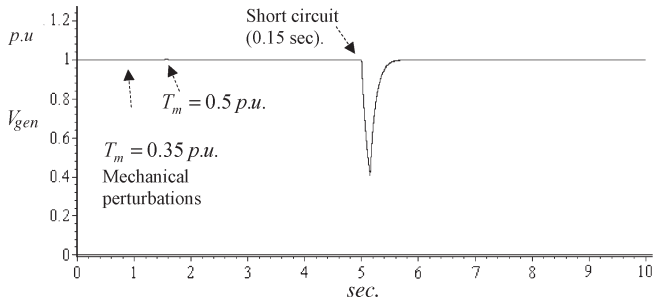

Fig. 6. Generator voltage affected by a 0.15-s short circuit (HOSM controller).

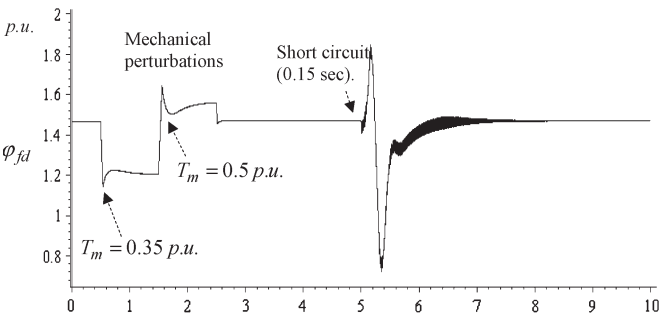

Fig. 7. Field flux linkage under mechanical perturbation and short circuit (HOSM controller).

field flux linkage reach a steady-state condition, exhibiting the stability of the closed-loop system (HOSM controller).

Test A.2—Step Changes in T_m and Three-Phase Short Circuit With Generator Parameter Variations: In the second test, the same perturbations as in the first test are applied but considering the most important parameter variations in generator L_{md} and L_{mq}. The solid line in Fig. 8 is the response of the proposed HOSM controller applied to the nominal plant, while the dotted and gray lines correspond to the plant parameter perturbations: The values of parameters L_{md} and L_{mq} experience variations of $\pm 40\%$, respectively, introducing variations of parameters a_{31}, a_{32}, a_{33}, c_{di}, and c_{qi}, where $i = 1, \ldots, 6$ in (7) and (8). We can observe that the angle δ converges to the steady-state value, and it is invariant with respect to the plant parameter variations.

Test A.3—Change in External Topology: In the third test, a step change in the equivalent external line reactance from 0.1 p.u. to 0.5 p.u. is applied at time $t = 3$ s. This is equivalent to break down four parallel external lines. From Fig. 9, it is clear that the HOSM controller is able to reject the external perturbation.

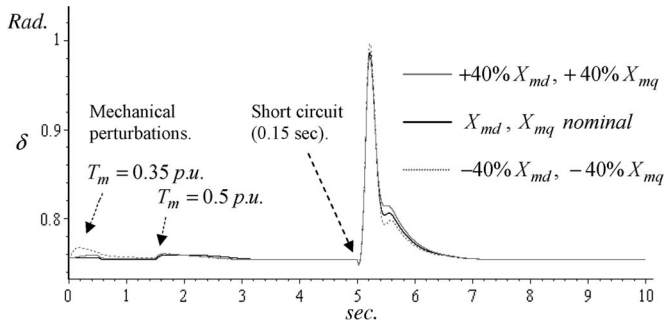

Fig. 8. Power angle performance during mechanical perturbation and short circuit, with a step change of L_{md} and L_{mq} (HOSM controller).

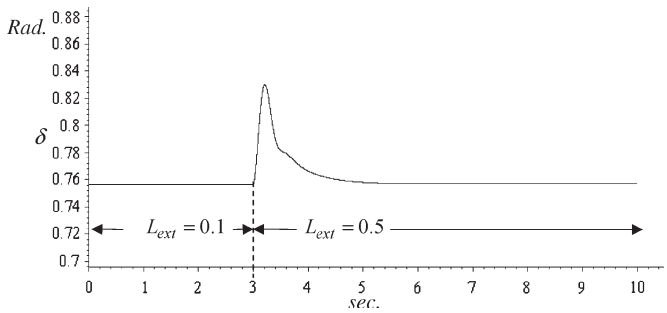

Fig. 9. Power angle performance during a step change in external line configuration (HOSM controller).

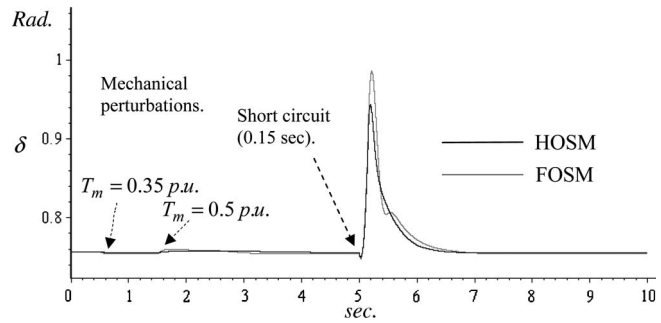

Fig. 10. Power angle performance: HOSM versus FOSM.

Test A.4—Step Changes in T_m and Three-Phase Short Circuit; HOSM controller Versus FOSM One: In the fourth test, the performance of the HOSM controller (solid line) is compared to the FOSM one (gray line in Figs. 10 and 13, and dotted line in Figs. 11 and 12). The events are the same as in the first set simulations. The transient behaviors of the power angle, rotor velocity, and control are shown in Figs. 10, 13–15, respectively (with black HOSM and gray FOSM), while the steady-state accuracy comparison for the power angle on smaller scales is shown in Figs. 11 and 12. The transient behavior, as well as steady-state performance comparison of two controllers, exhibits the clear advantage of the proposed HOSM controller.

Regarding the comparison of the controller behaviors (Figs. 14 and 15), it can be noted that the HOSM controller performs better than the FOSM one regarding the magnitudes of the transients caused by the disturbances (see Figs. 4–13). Fig. 15 shows distinct periods of control saturation that are not evident in Fig. 14 for the FOSM controller. The controller (36) gains, i.e., the parameters of the continuous switching

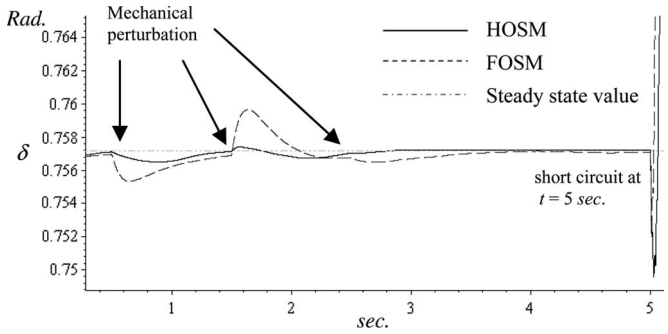

Fig. 11. Representation of Fig. 10 on a smaller scale, steady state for $0 \leq t < 5$ s.

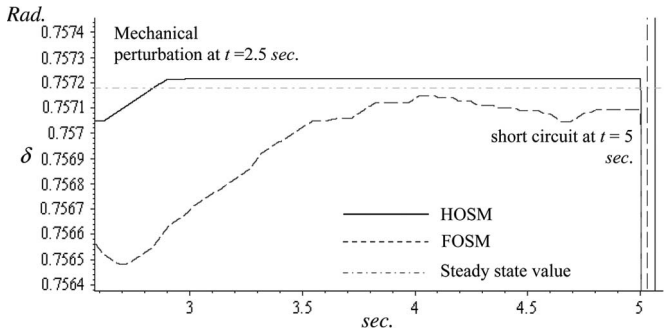

Fig. 12. Representation of Fig. 10 on a smaller scale, steady state for $2.5 \leq t < 5$ s.

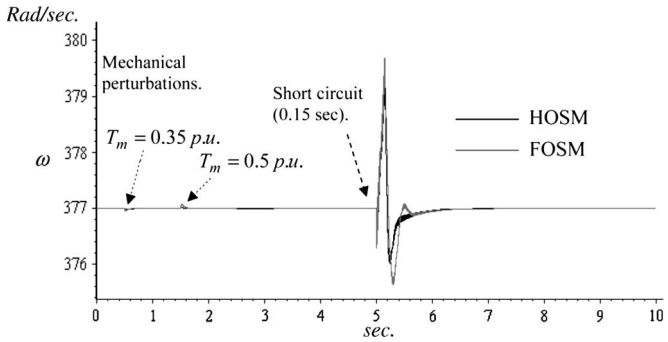

Fig. 13. Rotor velocity: HOSM versus FOSM.

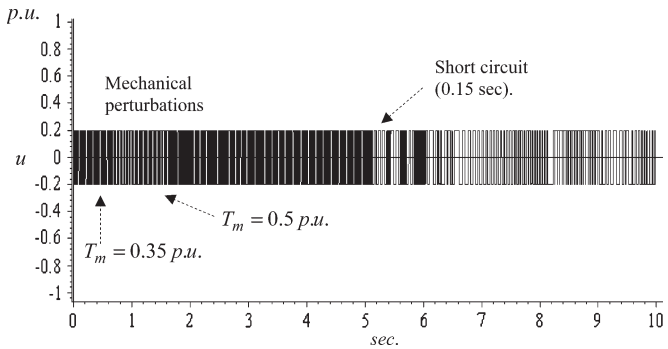

Fig. 14. Control input u under mechanical perturbation and short circuit (FOSM controller).

function $\psi_{2,3}(s_0, s_1, s_2)$, are larger than the parameters of the smooth switching function in the FOSM controller; therefore, the equivalent control magnitude during the application of the disturbances becomes much larger in the case of HOSM

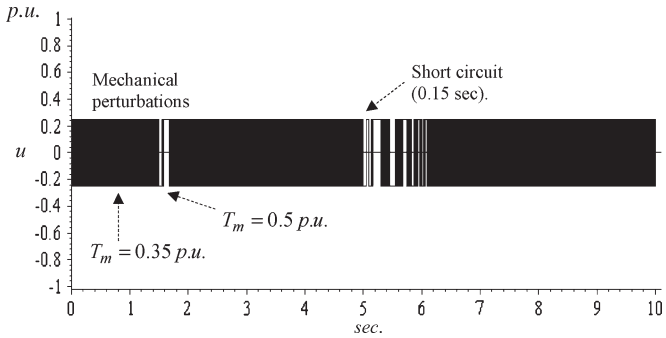

Fig. 15. Control input u under mechanical perturbation and short circuit (HOSM controller).

controller than in the case of FOSM one. This leads to the larger saturation period in the first case than in the second one.

On the other hand, the variables of the HOSM controller are faster than those in the FOSM one; moreover, the HOSM controller provides higher order finite-time convergence to the manifold $s_0 = 0$, while the FOSM controller ensures only asymptotic convergence to $s_0 = 0$. As a result, the switching frequency during SM and steady state in the system with HOSM controller (see Figs. 14 and 15) is higher than with the FOSM one. As it was mentioned before, the implementation of the HOSM control in the discrete time gives the precision $O(h^q)$, while the FOSM will give us just $O(h)$ precision.

VI. Conclusion

In this paper, a nonlinear excitation controller for a power system has been proposed. The simple control design was based on a combination of the block control and SM control techniques. In particular, the HOSM algorithm was applied to ensure chattering-free stability of closed-loop system in the presence of the unmodeled exciter system dynamics. The robust and high-accuracy performance of the designed controller was checked and confirmed by simulations. The performance comparison of two controllers, FOSM and HOSM, demonstrated the clear advantage of the proposed HOSM controller. The designed controller can be constituted instead of the existing PSS in a traditional structure as a supplementary loop to the main AVR. The proposed control methodology can be extended to multimachine systems.

Appendix

To derive the nonlinear transformation (15) which linearizes the nominal part of (12), the block control design technique [18], [23] is used, considering x_{i+1}, $i = 1, \ldots, r-1$ as a virtual control vector in each ith block of (12). The transformation procedure is outlined in the following steps.

Step 1) Let the fictitious control x_2 in the first block (12), rewritten as

$$\dot{z}_1 = f_1(x_1) + b_1(x_1)x_2 + g_1(x_1, t) - \dot{y}_{\text{ref}} \tag{A1}$$

be selected of the form

$$x_2 = b_1^{-1}(x_1)\left[-f_1(x_1) - k_1 z_1 + \dot{y}_{\text{ref}} + z_2\right] \tag{A2}$$

where z_2 is a new variable, and $k_1 > 0$. The first transformed block (A1) in new variables z_1 and z_2, with input (A2), has the desired form (16), i.e.,

$$\dot{z}_1 = -k_1 z_1 + z_2 + \tilde{g}_1(z_1, t).$$

Using (A2), the variable z_2 can be obtained as (15), i.e.,

$$z_2 = b_1^{-1}(x_1)x_2 + f_1(x_1) + k_1\varphi_1(x_1, t) - \dot{y}_{\text{ref}} \triangleq \varphi_2(\overline{x}_1, t).$$

Step i) At this stage, it is possible to show that we have, after $(i-1)$ steps, the transformed blocks of system (12) with the new variables $z_1, z_2, \ldots, z_{i-1}$ given by

$$\begin{aligned} \dot{z}_1 &= -k_1 z_1 + z_2 + \overline{g}_1(z_1, t) \\ &\vdots \\ \dot{z}_{i-1} &= -k_{i-1} z_{i-1} + z_i + \tilde{g}_{i-1}(\overline{z}_{i-1}, t) \end{aligned} \tag{A3}$$

with

$$z_i = \varphi_i(\overline{x}_i, t). \tag{A4}$$

Then, on the ith step of the transformation procedure, we will have the transformed ith block with a new state vector z_i similar to (A3). To carry this out, taking the derivative of (A4) along the trajectories of (12) results in

$$\dot{z}_i = \tilde{f}_i(\overline{x}_i) + \tilde{b}_i(\overline{x}_i)x_{i+1} + \tilde{g}_i(\overline{x}_i, t) \tag{A5}$$

where

$$\tilde{f}_i = \sum_{j=1}^{i-1}\left[\frac{\partial\varphi_i}{\partial x_j}f_j + b_j x_{j+1}\right] + \frac{\partial\varphi_i}{\partial x_i}f_i + \frac{\partial\varphi_i}{\partial t}$$

$$\tilde{g}_i = \sum_{j=1}^{i}\frac{\partial\varphi_i}{\partial x_j}g_j \qquad \tilde{b}_i = \tilde{b}_{i-1}b_i.$$

The fictitious control vector x_{i+1} in (A5) can be selected similar to (A2), of the form

$$x_{i+1} = \tilde{b}_i^{-1}(\overline{x}_i)\left[-\tilde{f}_i(\overline{x}_i) - k_i z_i + z_{i+1}\right] \tag{A6}$$

where $-k_i z_i$ is a desired linear dynamics for z_i. Thus, (A5) with (A6) takes the same form as (A3), i.e.,

$$\dot{z}_i = -k_i z_i + z_{i+1} + \tilde{g}_i(\overline{z}_i, t).$$

Using (A6) we can obtain the recursive transformation (15), i.e.,

$$z_{i+1} = \tilde{b}_i(\overline{x}_i)x_{i+1} - \tilde{f}_i(\overline{x}_i) - k_i z_i.$$

Step r) On the last step, calculating the time derivative of $z_r = \varphi_r(\overline{x}_r)$ gives the last block

$$\dot{z}_r = \tilde{f}_r(\overline{z}_r, \overline{x}_{r+1}) + \tilde{b}_r(\overline{z}_r, \overline{x}_{r+1})u + \tilde{g}_r(\overline{z}_r, \overline{x}_{r+1}, t)$$

where

$$\tilde{f}_r = \sum_{j=1}^{r-1}\left[\frac{\partial\varphi_r}{\partial x_j}f_j + b_j x_{j+1}\right] + \frac{\partial\varphi_r}{\partial x_i}f_i + \frac{\partial\varphi_r}{\partial t}$$

$$\tilde{b}_r = \tilde{b}_{r-1}b_r \qquad \tilde{g}_r = \sum_{j=1}^{r}\frac{\partial\varphi_r}{\partial x_j}g_j$$

thus, transformation (14) and (15) reduces the system (12) and (13) to (16).

REFERENCES

[1] G. P. Kundur, *Power System Stability and Control*. New York: McGraw-Hill, 1994.

[2] J. Machowski, S. Robak, J. W. Bialek, J. R. Bumby, and N. Abi-Samra, "Decentralized stability-enhancing control of synchronous generator," *IEEE Trans. Power Syst.*, vol. 15, no. 4, pp. 1336–1345, Nov. 2000.

[3] P. W. Sauer and M. A. Pai, *Power System Dynamics and Stability*. Englewood Cliffs, NJ: Prentice-Hall, 1998.

[4] A. Ghandakly and P. Idowu, "Design of a model reference adaptive stabilizer for the exciter and governor loops of power generators," *IEEE Trans. Power Syst.*, vol. 5, no. 3, pp. 887–893, Aug. 1990.

[5] S. Mohagheghi, Y. del Valle, G. K. Venayagamoorty, and R. G. Harley, "A proportional-integrator type adaptive critic design-based neurocontroller for a static compensator in multimachine power systems," *IEEE Trans. Ind. Electron.*, vol. 54, no. 1, pp. 86–96, Feb. 2007.

[6] T. Hiyama, Y. Ueki, and H. Andou, "Integrated fuzzy logic generator controller for stability enhancement," *IEEE Trans. Energy Convers.*, vol. 12, no. 4, pp. 400–406, Dec. 1997.

[7] M. Lown, E. Swidenbank, and B. W. Hogg, "Adaptive fuzzy logic control of a turbine generator system," *IEEE Trans. Energy Convers.*, vol. 12, no. 3, pp. 394–399, Dec. 1997.

[8] Y. Hsu and L. Chen, "Tuning of power system stabilizers using an artificial neural network," *IEEE Trans. Energy Convers.*, vol. 6, no. 4, pp. 612–619, Dec. 1991.

[9] P. Shamsollahi and O. P. Malik, "An adaptive power system stabilizer using on-line trained neural network," *IEEE Trans. Energy Convers.*, vol. 12, no. 4, pp. 382–387, Dec. 1997.

[10] S. Jain, F. Khorrami, and I. Fardanesh, "Adaptive nonlinear excitation control of power systems with unknown interconnections," *IEEE Trans. Control Syst. Technol.*, vol. 2, no. 4, pp. 436–446, Dec. 1994.

[11] L. Gao, L. Chen, Y. Fan, and H. Ma, "DFL—Nonlinear control design with applications in power systems," *Automatica*, vol. 28, pp. 975–979, 1992.

[12] W. Mielczarski and A. M. Zajaczkowski, "Nonlinear field voltage control of a synchronous generator using feedback linearization," *Automatica*, vol. 30, no. 10, pp. 1625–1630, Oct. 1994.

[13] V. I. Utkin, J. Guldner, and J. Shi, *Sliding Mode Control in Electromechanical System*. London, U.K.: Taylor & Francis, 1999.

[14] K. Abidi and A. Šabanovic, "Sliding-mode control for high-precision motion of a piezostage," *IEEE Trans. Ind. Electron.*, vol. 54, no. 1, pp. 629–637, Feb. 2007.

[15] W.-F. Xie, "Sliding-mode-observer-based adaptive control for servo actuator with friction," *IEEE Trans. Ind. Electron.*, vol. 54, no. 3, pp. 1517–1527, Jun. 2007.

[16] A. V. Topalov, G. L. Cascella, V. Giordano, F. Cupertino, and O. Kaynak, "Sliding mode neuro-adaptive control of electric drives," *IEEE Trans. Ind. Electron.*, vol. 54, no. 1, pp. 671–679, Feb. 2007.

[17] Y. Yildiz, A. Šabanovic, and K. Abidi, "Sliding-mode neuro-controller for uncertain systems," *IEEE Trans. Ind. Electron.*, vol. 54, no. 3, pp. 1676–1685, Jun. 2007.

[18] A. G. Loukianov, J. M. Cañedo, V. I. Utkin, and J. Cabrera-Vázquez, "Discontinuous controller for power system: Sliding-mode block control approach," *IEEE Trans. Ind. Electron.*, vol. 51, no. 2, pp. 340–353, Apr. 2004.

[19] H. Huerta, A. G. Loukianov, and J. M. Canedo, "Multimachine power-system control: Integral-SM approach," *IEEE Trans. Ind. Electron.*, vol. 56, no. 6, pp. 2229–2236, Jun. 2009.

[20] I. Boiko, L. Fridman, A. Pisano, and E. Usai, "Analysis of chattering in systems with second-order sliding modes," *IEEE Trans. Autom. Control*, vol. 52, no. 11, pp. 2085–2102, Nov. 2007.

[21] L. Fridman, "An averaging approach to chattering," *IEEE Trans. Autom. Control*, vol. 46, no. 8, pp. 1260–1265, Aug. 2001.
[22] L. Fridman, "Singularly perturbed analysis of chattering in relay control systems," *IEEE Trans. Autom. Control*, vol. 47, no. 12, pp. 2079–2084, Dec. 2002.
[23] A. G. Loukianov, "Robust block decomposition sliding mode control design," *Math. Probl. Eng.*, vol. 8, no. 4/5, pp. 349–365, 2002.
[24] G. Bartolini, A. Punta, A. Pisano, and E. Usai, "A survey of applications of second-order sliding mode control to mechanical systems," *Int. J. Control*, vol. 76, no. 9/10, pp. 875–892, Jun. 2003.
[25] A. Levant, "Higher-order sliding modes, differentiation and output-feedback control," *Int. J. Control*, vol. 76, no. 9/10, pp. 924–941, Jun. 2003.
[26] A. Levant, "Homogeneity approach to high-order sliding mode design," *Automatica*, vol. 41, no. 5, pp. 823–830, May 2005.
[27] G. Bartolini, A. Ferrara, and E. Usai, "Chattering avoidance by second-order sliding mode control," *IEEE Trans. Autom. Control*, vol. 43, no. 2, pp. 241–246, Feb. 1998.
[28] A. Levant, "Quasi-continuous high-order sliding-mode controllers," *IEEE Trans. Autom. Control*, vol. 50, no. 11, pp. 1812–1816, Nov. 2005.
[29] S. Rao, M. Buss, and V. Utkin, "Simultaneous state and parameter estimation in induction motors using first- and second-order sliding modes," *IEEE Trans. Ind. Electron.*, vol. 56, no. 9, pp. 3369–3376, Sep. 2009.
[30] M. Defoort, F. Nollet, T. Floquet, and W. Perruquetti, "A third-order sliding-mode controller for a stepper motor," *IEEE Trans. Ind. Electron.*, vol. 56, no. 9, pp. 3337–3346, Sep. 2009.
[31] M. Tanelli, C. Vecchio, M. Corno, A. Ferrara, and S. M. Savaresi, "Traction control for ride-by-wire sport motorcycles: A second-order sliding mode approach," *IEEE Trans. Ind. Electron.*, vol. 56, no. 9, pp. 3347–3356, Sep. 2009.
[32] A. Estrada and L. Fridman, "Quasi-continuous HOSM control for systems with unmatched perturbations," in *Proc. IEEE Workhop VSS*, 2008, pp. 179–184.
[33] R. H. Park, "Two-reaction theory of synchronous machines—Generalized methods of analysis—Part I," *AIEE Trans.*, vol. 48, pp. 716–727, 1933.
[34] R. H. Park, "Two-reaction theory of synchronous machines—Generalized methods of analysis—Part II," *AIEE Trans.*, vol. 52, pp. 352–355, 1929.
[35] A. W. Rankin, "Per-unit impedance of synchronous machines," *AIEE Trans.*, vol. 64, pp. 569–573, 1945.
[36] P. C. Krause, *Analysis of Electric Machinery*. New York: McGraw-Hill, 1987.
[37] "Computer representation of excitation systems," *IEEE Trans. Power App. Syst.*, vol. PAS-87, no. 6, pp. 1460–1464, Jun. 1988.
[38] A. Soto-Cota, L. M. Fridman, A. G. Loukianov, and J. M. Cañedo, "Variable structure control of synchronous generator: Singularly perturbed analysis," *Int. J. Control*, vol. 79, no. 1, pp. 1–13, Jan. 2006.
[39] M. Krstic, I. Kanellakopoulos, and P. Kokotovic, *Nonlinear and Adaptive Control Design*. New York: Wiley-Interscience, 1995.
[40] A. Isidori, *Nonlinear Control Systems*. London, U.K.: Springer-Verlag, 1992.

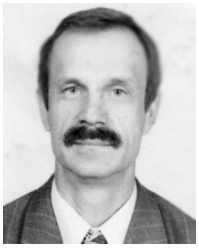

Alexander G. Loukianov (M'06) received the Dipl. Eng. degree from Polytechnic Institute, Moscow, Russia, in 1975, and the Ph.D. degree in automatic control from the Institute of Control Sciences, Russian Academy of Sciences, Moscow, in 1985.

From 1978 to 1997, he was with the Institute of Control Sciences, Russian Academy of Sciences. Since April 1997, he has been with the Advanced Studies and Research Center, National Polytechnic Institute (CINVESTAV-IPN), Guadalajara, México. He has published more than 150 technical papers in international journals, books, and conferences and has served as a Reviewer for different international journals and conferences. He is an Associate Editor of the *International Journal of Control Theory and Applications*. His research interests include nonlinear robust control and variable structure systems with sliding modes as applied to electric drives and power system control, robotics, and automotive control.

José M. Cañedo (M'77) was born in Mazatlán, México, in 1950. He received the B.S. degree in electrical engineering power systems from Guadalajara University, Guadalajara, México, in 1971, the M.S. degree from the National Polytechnic Institute of México, México City, México, in 1980, and the Ph.D. degree from the Moscow Power Institute, Moscow, Russia, in 1985.

From 1988 to 1994, he was a Researcher with the Federal Power Commission of México. Since 1997, he has been with the Advanced Studies and Research Center, National Polytechnic Institute (CINVESTAV-IPN), Guadalajara, as a Professor of Electrical Engineering Graduate Programs. His research interests include nonlinear robust control of power systems and electric machines.

Leonid M. Fridman (M'09) received the M.S. degree in mathematics from Kuibyshev (Samara) State University, Samara, Russia, in 1976, the Ph.D. degree in applied mathematics from the Institute of Control Sciences, Russian Academy of Sciences, Moscow, Russia, in 1988, and the Dr.Sci. degree in control science from Moscow State University of Mathematics and Electronics, Moscow, in 1998.

From 1976 to 1999, he was with the Department of Mathematics, Samara State Architecture, Samara. From 2000 to 2002, he was with the Department of Postgraduate Study and Investigations, Chihuahua Institute of Technology, Chihuahua, México. Since 2002, he has been with the Department of Control and Robotics, Division of Electrical Engineering of Engineering Faculty, National Autonomous University of Mexico, México City, México. He is an Associate Editor of the *International Journal of System Science*. He is an Editor of three books and five special issues on sliding-mode (SM) control. He has published over 200 technical papers. His research interests include variable structure systems and singular perturbations.

Prof. Fridman is an Associate Editor of the Conference Editorial Board of IEEE Control Systems Society and a member of the Technical Committee on Variable Structure Systems and SM Control, IEEE Control Systems Society.

Adolfo Soto-Cota (S'02–M'08) was born in 1972. He received the M.S. and Ph.D. degrees in automatic control from the Advanced Studies and Research Center, National Polytechnic Institute (CINVESTAV-IPN), Guadalajara, México, in 2000 and 2004, respectively.

From 1995 to 1997, he was with Sony, Tijuana, México. Since August 1999, he has been with the Instituto Tecnológico de Sonora (Sonora Institute of Technology), Obregón, México. His research interests include variable structure systems with sliding modes, singular perturbations, electric drives, electric machinery, and power system control.